Epitaxial Thin Film Growth of Perovskite Hydrides MLiH$_3$ (M : Sr, Ba) for The Study of Intrinsic Hydride-Ion Conduction

Erika Fukushi[1], Fumiya Mori[1], Kota Munefusa[1], Takayuki Harada[2] and Hiroyuki Oguchi[1]*

[1]Department of Applied Chemistry, Graduate School of Engineering and Science, Shibaura Institute of Technology, 3-7-5 Toyosu, Koto-ku, Tokyo, Japan

[2]Research Center for Materials Nanoarchitectonics (MANA), National Institute for Materials Science, 1-1 Namiki, Tsukuba-shi, Ibaraki, Japan

Perovskite hydride, Hydride-ion conduction, Epitaxial thin film, Radical hydrogen

ABSTRACT: Perovskite hydrides, with their excellent elemental substitution ability, are ideal materials for stimulating research on the physical properties of hydrides through material design. For the material design, it is necessary to correctly understand the physical property of perovskite hydrides and to elucidate its origin. In this regard, studies using single-crystal epitaxial thin films that enable observation of the intrinsic properties of the materials are effective. In this study, MLiH$_3$ (M : Sr, Ba) epitaxial thin films were synthesized by radical hydrogen reactive infrared laser deposition, which is a highly efficient method for growing hydride phases using the high reactivity of radical hydrogen. Furthermore, the intrinsic hydride-ion conductivity, which is not affected by grain boundaries, was successfully determined for SrLiH$_3$ using the synthesized epitaxial thin film. These results established the basic technology for the epitaxial growth of perovskite hydrides and paved the way for the research on the control of physical properties by elemental substitution in perovskite hydrides.

1. Introduction

Hydrides are a series of compounds in which a negatively charged hydride-ion (H^-) is bonded to other elements. Hydrides are attractive targets for the development of functional materials because they can often exhibit special properties derived from hydrogen. Examples of hydrogen-derived properties include hydrogen storage properties,[1, 2] high-temperature superconductivity,[3, 4, 5, 6]and hydride-ion conduction.[7, 8] These properties have the potential to be used to develop energy-saving materials such as superconducting power cables. The development of energy devices such as new types of batteries and fuel cells using hydride-ion conduction is also expected. Therefore, hydrides are materials that could revolutionize the energy field.

Perovskite hydrides[9, 10, 11, 12, 13] are ideal materials for stimulating research on the physical properties of hydrides. This is because perovskite hydrides, which have a perovskite structure with high elemental substitution ability, are expected to create and improve various physical properties. In fact, in the perovskite hydride $AB(BH_4)_3$, the electronic structures and luminescence properties were changed by lattice deformation through the combination of various elements.[14] Furthermore, in the perovskite hydride MLiH$_3$ (M : Ba, Sr), the hydride-ion conductivity were increased by substituting divalent elements M with monovalent elements.[15]

To accelerate research on perovskite hydrides, accurate characterization of physical properties is necessary since it can provide us clues to clarify the origin of physical properties. However, accurate characterization of physical properties has often been difficult in perovskite hydride research to date. For example, in the case of MLiH$_3$ introduced earlier, the experiments were conducted on a powder sample with a high percentage of grain boundaries, so the impedance measurement data was strongly affected by the grain boundaries, which obscured the original hydride-ion conductivity of the MLiH$_3$ crystal.

One effective means of accurately characterizing the intrinsic properties of a material is to use epitaxial thin films,[16] which are single-crystalline thin films. Fortunately, research on epitaxial thin films of hydrides, which had previously been reported in only three cases,[17, 18, 19] has recently been revitalized, and the number of reported syntheses is increasing. So far, as epitaxial thin films, LiH has been synthesized by vapor-liquid-solid growth[20] and pulsed laser deposition,[21] TiH$_2$ by pulsed laser deposition,[22] and TiH$_2$ MgH$_2$, YH$_2$, NbH$_3$ and EuH$_2$ by sputtering,[23, 24, 25, 26, 27] respectively. In addition to these, the complex hydrides LiBH$_4$ and NaBH$_4$ with molecular $[BH_4]^{2-}$ complex anions in their structures have been synthesized by infrared laser evaporation.[28, 29] However, these are all binary or quasi-binary hydrides, and there have been no reports of epitaxial thin film synthesis of perovskite hydrides, which are ternary hydrides that are expected to be more difficult to synthesize than binary hydrides.

In this study, we firstly determine the synthesis temperature suitable for MLiH$_3$ epitaxial thin film synthesis. Next, the effect of radical hydrogen on metal residues in MLiH$_3$ thin films will be examined. Epitaxial thin film synthesis is then performed under conditions determined to be appropriate based on the results of these investigations. Finally,

the epitaxial films will be used to evaluate the intrinsic hydride-ion conductivity of $SrLiH_3$.

2. EXPERIMENTAL SECTION

MLiH_3 epitaxial thin films were synthesized by a radical hydrogen reactive infrared laser deposition method that we developed for this study (Figure 1). This method is an improvement version of the infrared laser evaporation, which is a powerful method for organic thin film synthesis[28, 29, 30]. The most outstanding feature of the new technique is that deposition can be carried out in a radical hydrogen atmosphere, which strongly promotes the reaction between the metal and hydrogen. Therefore, it is expected to synthesize single-phase hydride thin films by completely hydrogenating the metal that tends to remain in the film. The films were deposited in an ultra-high vacuum chamber with a back pressure of less than 1.0×10^{-8} Torr. Radical hydrogen was generated by flowing H_2 gas at 1.0×10^{-2} Torr through a high-temperature tungsten filament attached inside the chamber. The substrates used in this study were $MgAl_2O_4$(100) (lattice mismatch is -0.5 % for $BaLiH_3$ and -5.2 % for $SrLiH_3$) and $LaAlO_3$(100) (lattice mismatch is +0.3 % for $SrLiH_3$). The substrate temperature during deposition was set in the range of 100 - 170 °C to promote film crystallization and prevent hydrogen desorption from the films. The target was a disk-shaped pellet with a diameter of 20 mm and a thickness of about 1.5 mm, obtained by uniaxially pressurizing a powder mixture of MH_2 and LiH at a molar ratio of 1:1. A non-focused continuous wave infrared laser (wavelength 808 nm) (LIMO32-F-400-DL808-EX2024) was used to heat the target. The target was rotated at a speed of approximately 60 - 120 rpm to ensure homogeneous heating and to stabilize the deposition rate. The target-substrate distance was about 60 mm and the deposition rate was 0.5 - 1.0 Å / sec.

The crystallinity and orientation of the thin films were evaluated by X-ray diffraction (XRD) measurements (SmartLab, Rigaku and Empyrean 3, Malvern). To prevent sample degradation during the measurements, Cu with a thickness of 0.5 μm to 1 μm was deposited on the films as a protective layer. Surface conditions were evaluated with an optical microscope (ME-LUX2, KYOWA OPTICAL CO.), scanning electron microscope (SEM) (JSM-7800F, JEOL), and atomic force microscope (AFM) (MultiMode 8, Bruker AXS). Film thickness was determined by cross-sectional observation by SEM. In-plane hydride-ion conductivity was evaluated using an electrochemical impedance measurement system (SP-150, Biologic) in a vacuum chamber (back pressure: 1×10^{-7} Torr). The measurement temperature range was from room temperature to 200 °C, and the applied frequency range was 1 Hz ~ 1 MHz. Comb-shaped electrodes made by Mo were deposited at room temperature in a vacuum chamber using a patterned shadow mask (Figure S1). To prevent degradation of the thin films, all of the above experimental manipulations and characterizations were performed in a non-air-exposure environment.

3. RESULTS AND DISCUSSION

Initially, we searched for a suitable synthesis temperature for the growth of $BaLiH_3$ thin films by radical hydrogen reactive infrared laser evaporation. The H_2 gas pressure in the

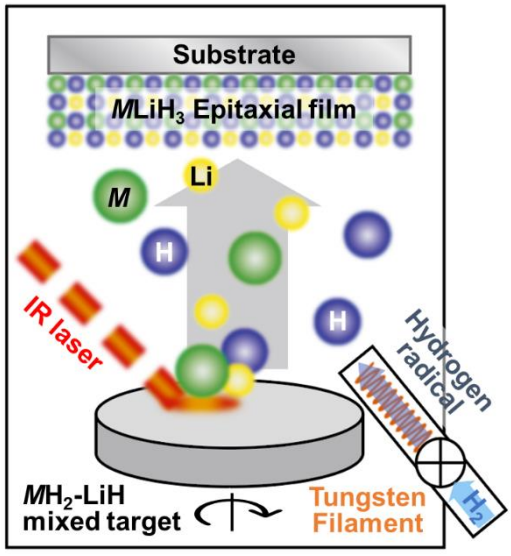

Figure 1. Schematic of *M*LiH_3 epitaxial thin film synthesis by radical hydrogen reactive infrared laser evaporation. On the substrate, metal *M* and metal Li react with hydrogen to grow *M*LiH_3 phase. Hydrogen supplied by the *M*H_2-LiH target are used in film growth, too.

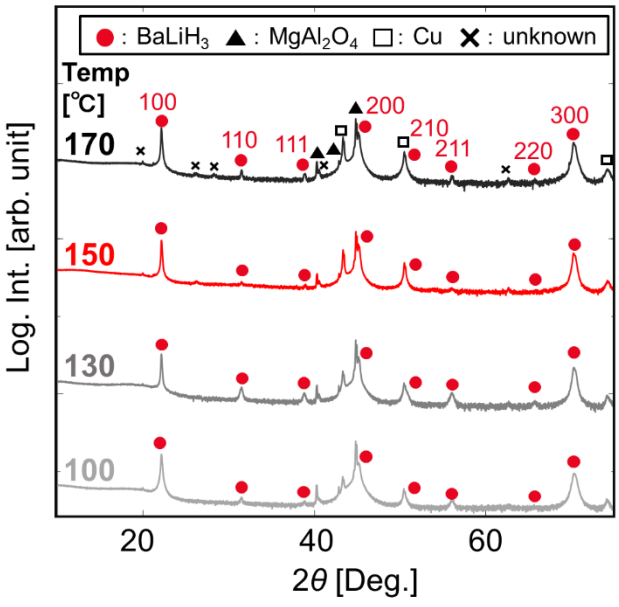

Figure 2. The $2\theta/\theta$ XRD patterns of $BaLiH_3$ films deposited at 100, 130, 150, and 170 °C. The vertical axis is offset to make it easier to see the patterns for different temperatures.

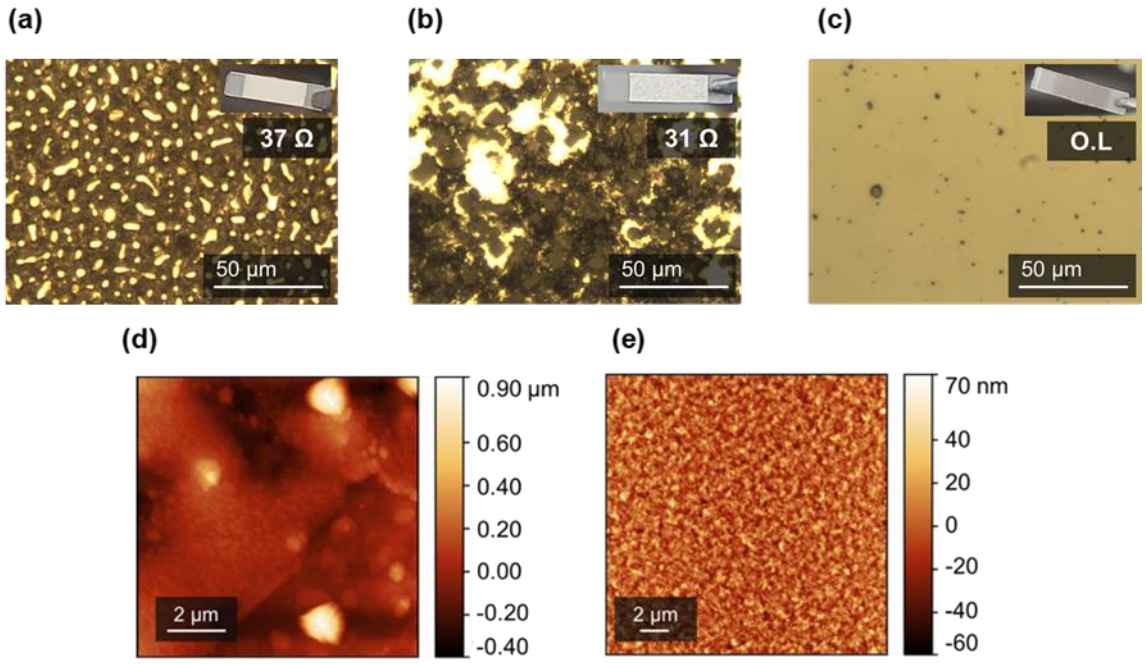

Figure 3. Optical microscope images of $BaLiH_3$ thin films synthesized under (a) H_2 gas, (b) radical hydrogen gas with low concentration (The W filament temperature T_f = 800 °C), and (c) radical hydrogen gas with high concentration T_f = 2000 °C). For (a) – (c), hydrogen gas pressure P_{H2} was set to 1.0 × 10^{-2} Torr. The upper right of these figures shows a photograph of the sample and the film resistance measured with a multimeter. (d) AFM image of the film in (b). (e) AFM image of the film in (c).

radical hydrogen generator was set to 1.0 × 10^{-2} Torr and the W filament temperature T_f to 800 °C. Figure 2 shows $2\theta/\theta$ XRD diffraction patterns of $BaLiH_3$ thin films grown on $MgAl_2O_4$(100) substrates at temperatures between 100 and 170 °C. $BaLiH_3$-derived diffraction peaks were observed at all temperatures. The most clearly observed peaks were h00 (h = 1, 2, 3) diffraction ones. In addition to those peaks, the films synthesized at 100 ºC and 130 ºC also exhibited 110 (2θ = 31.5°), 111 (2θ = 38.8°), 210 (2θ = 50.5°), 211 (2θ = 56.0°), and 220 (2θ = 65.7°) diffraction peaks. At these temperatures, orientation was incomplete, probably because the crystal growth rate was not fast enough. At a deposition temperature of 150 °C, all but the diffraction peaks from the (h00) plane was very small, and a film with almost (100) orientation was obtained. However, when the temperature was further increased to 170 °C, diffraction peaks other than those from the (h00) plane became prominent again, suggesting a decrease in orientation. It may due to hydrogen desorption from the film, causing compositional deviations that distorted the crystals, resulting in a decrease in orientation. Based on these results, we concluded that 150 °C was appropriate for $BaLiH_3$ film deposition.

Next, to verify the effect of radical hydrogen on $BaLiH_3$ deposition, films were deposited when H_2 and radical hydrogen H gases were used as the reaction gas. In the latter case, amount of radical hydrogen was changed by changing the W filament temperature T_f in the radical hydrogen generator to 800 °C and 2000 °C. The experiment at T_f = 2000 °C was expected to generate a larger amount of radical hydrogen than at T_f = 800 °C.[31 32] For all three cases, H_2 gas pressure flown into the chamber was 1.0 × 10^{-2} Torr. $MgAl_2O_4$(100) was used as the substrate, and the substrate temperature was set at 150 °C during deposition. Figure 3 (a)-(c) shows optical microscope images of the films deposited under each condition. According to theoretical calculations,[9, 10, 11, 33] a band gap of the $BaLiH_3$ is 1 – 4 eV and thus it should be transparent. However, the films synthesized with H_2 and radical hydrogen (T_f = 800 °C) were opaque and shiny. When these films were observed under a microscope, light-reflecting areas that appeared to be Ba metal or Li metal were dispersed all over the observed image. The presence of metal was also confirmed by the fact that the resistance of these films shown in the upper right corner of each figure was less than 40 Ω. XRD $2\theta/\theta$ patterns of these films (Figure S2) showed diffraction peaks attributed to $BaLiH_3$, suggesting that the films were synthesized as a mixture of $BaLiH_3$ and metal phases. In contrast, the film synthesized under radical hydrogen (T_f = 2000 °C) was almost transparent, and the light-reflecting areas disappeared from the microscopic images, suggesting that the entire film was $BaLiH_3$. For this sample, the resistance was above the multimeter's measurement range. These results indicate that a nearly single-phase $BaLiH_3$ film with no metal contamination could be obtained by supplying a large amount of radical hydrogen to the film.

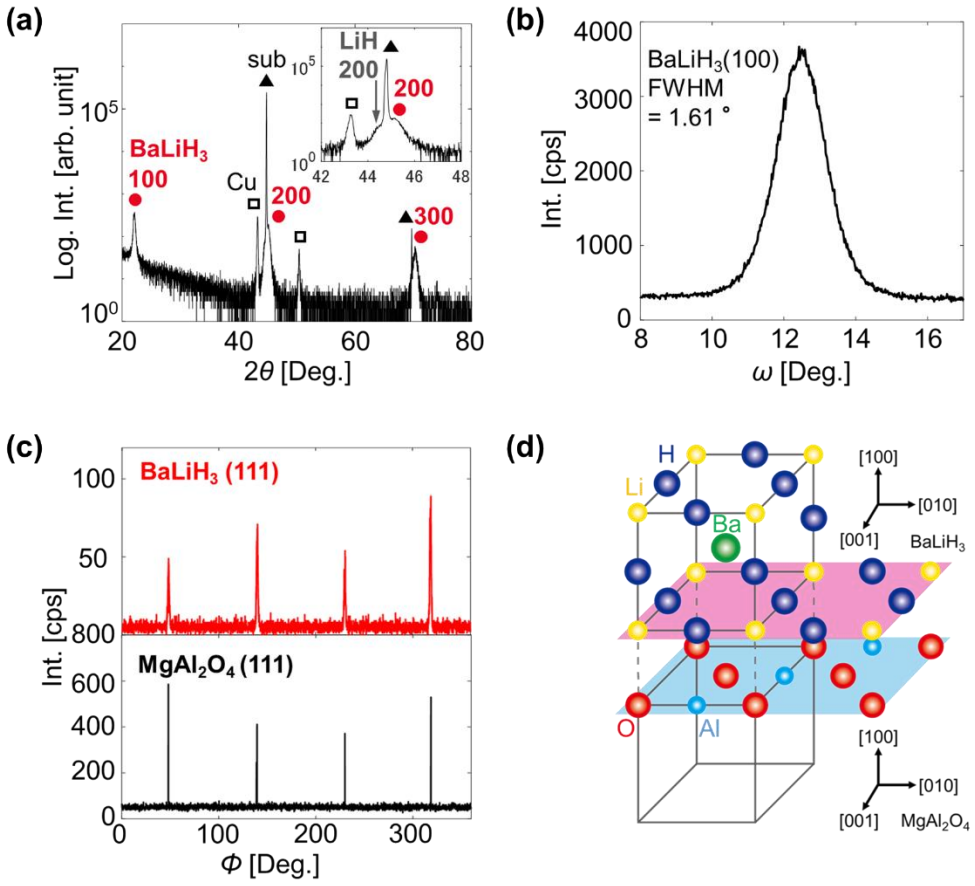

Figure 4. (a) $2\theta/\theta$ XRD diffraction pattern and (b) XRD rocking curve of $BaLiH_3$ thin film synthesized under optimal conditions. In the inset of (a), the area around the LiH 200 diffraction peak is enlarged. (c) φ scan pattern of a 111diffraction plane for $BaLiH_3$ thin film and $MgAl_2O_4$ substrate. (d) Atomic arrangement of the epitaxial thin film on the substrate expected from the results of (a) and (b).

AFM observations (Fig. 3(d) and (e)) of these films showed that high concentrations of radical hydrogen also contributed to the improvement of the flatness of the $BaLiH_3$ film. At T_f = 800 °C, the RMS average roughness of the entire image was as high as about 160 nm due to the scattered islands with diameters of 1 - 2 μm and heights of up to about 1 μm. On the other hand, at T_f = 2000 °C, the islands disappeared from the surface, resulting in a decrease in RMS average roughness to 13 nm.

The $BaLiH_3$ epitaxial thin film was successfully grown on a $MgAl_2O_4$(100) substrate under the conditions (substrate temperature 150 °C, P_{H2} = 1.0 × 10^{-2} Torr, T_f = 2000 °C) that yielded a flat, nearly single-phase $BaLiH_3$ film. Figure 4(a) shows the XRD $2\theta/\theta$ diffraction pattern. The h00 diffraction peaks of $BaLiH_3$ are the only peaks observed except for the substrate and the Cu protective layer, indicating that the $BaLiH_3$ epitaxial film is almost a single

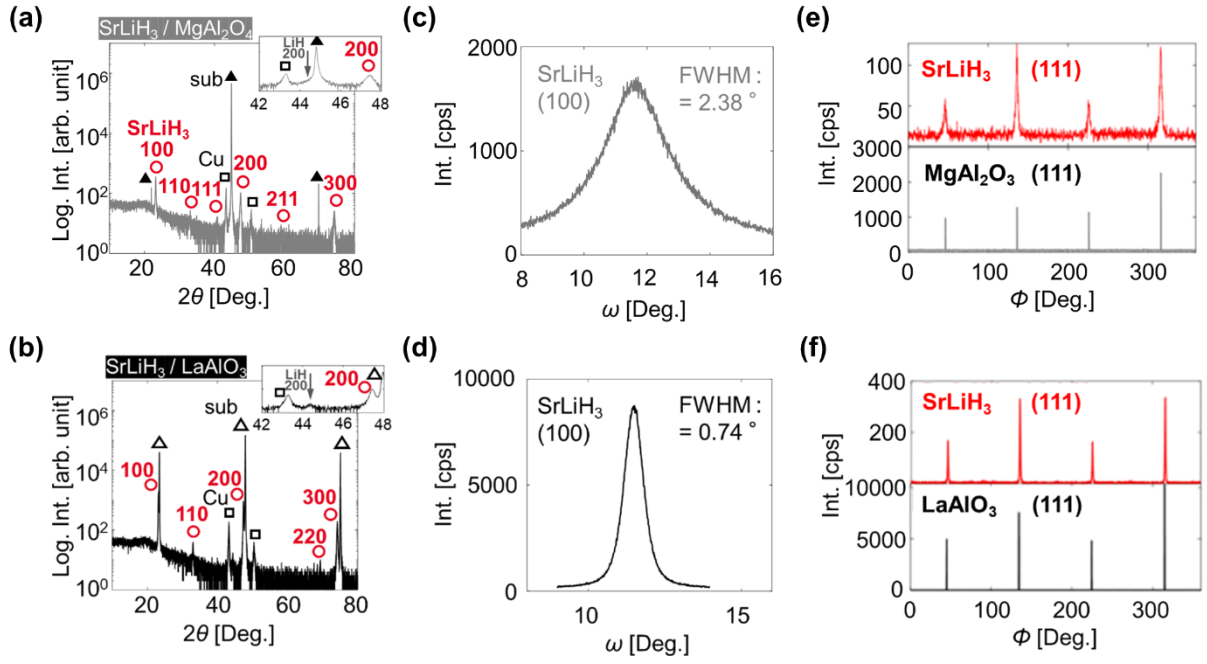

Figure 6. A set of XRD measurements for the $SrLiH_3$ films grown on a $MgAl_2O_4$ substrate ((a), (c), (e)) and a $LaAlO_3$ substrate ((b), (d), (f)). (a), (b) The XRD $2\theta/\theta$ patterns. Inset shows magnified view around LiH 200 diffraction peak. (c), (d) XRD rocking curves. (e), (f) XRD φ scan patterns.

phase film with a (100) orientation. A shoulder peak on the side of the 200 diffraction peak of $BaLiH_3$ suggesting the presence of small amount of LiH. The rocking curve FWHM of the $BaLiH_3$ 100 diffraction was 1.61°(Figure 4(b)). This FWHM value is relatively large when it is compared with other epitaxial films of hydrides.[20, 21, 24, 27, 28, 29] Possibly the oxide substrate surface was reduced and roughened by highly reductive radical hydrogen and crystallinity of the $BaLiH_3$ was lowered. The XRD φ scan shows 111 diffraction peaks at the same rotation angle for the film and substrate, indicating that the in-plane epitaxial relationship is $[001]_{BaLiH3} \parallel [001]_{sub}$ (Figure 4(c)(d)).

Cross-sectional SEM observations and energy dispersive spectroscopy (EDS) measurements of the $BaLiH_3$ epitaxial film indicated that it was a dense film of almost constant thickness and that there was almost no elemental diffusion between the film and the substrate. These characteristics make these films suitable for accurate evaluation of hydride-ion conduction. Figure 5 shows a cross-sectional SEM image of a $BaLiH_3$ epitaxial film prepared by cracking a $MgAl_2O_4$(100) substrate after growth of the film. The film thickness was about 1 μm at all positions on the substrate. In the EDS elemental mapping, Ba was detected only at the location of the film in the SEM image, and other elements (O, Mg, Al) were detected only at the location of the substrate.

The synthesis of $SrLiH_3$ was performed under the same conditions that produced high-quality epitaxial $BaLiH_3$ films, and high-quality $SrLiH_3$ epitaxial films were also successfully obtained. Figure 6(a) and (b) show XRD $2\theta/\theta$ diffraction patterns of samples grown on two different substrates ($MgAl_2O_4$ and $LaAlO_3$). $SrLiH_3$-derived diffraction peaks were observed on both substrates. Comparing two samples,

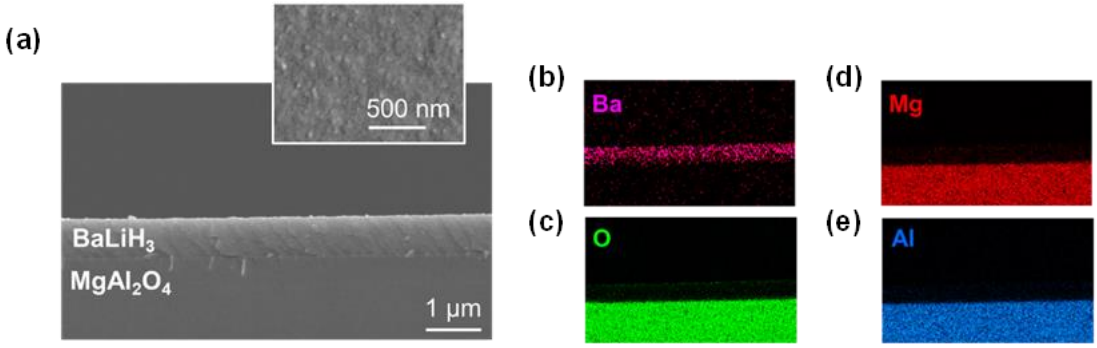

Fig. 5 A cross sectional SEM image (a) and EDS elemental mappings for (b) Ba, (c) O, (d) Mg, and (e) Al of a $BaLiH_3$ epitaxial thin film grown on a $MgAl_2O_4$(100) substrate. Inset in (a) shows a surface SEM image of this film.

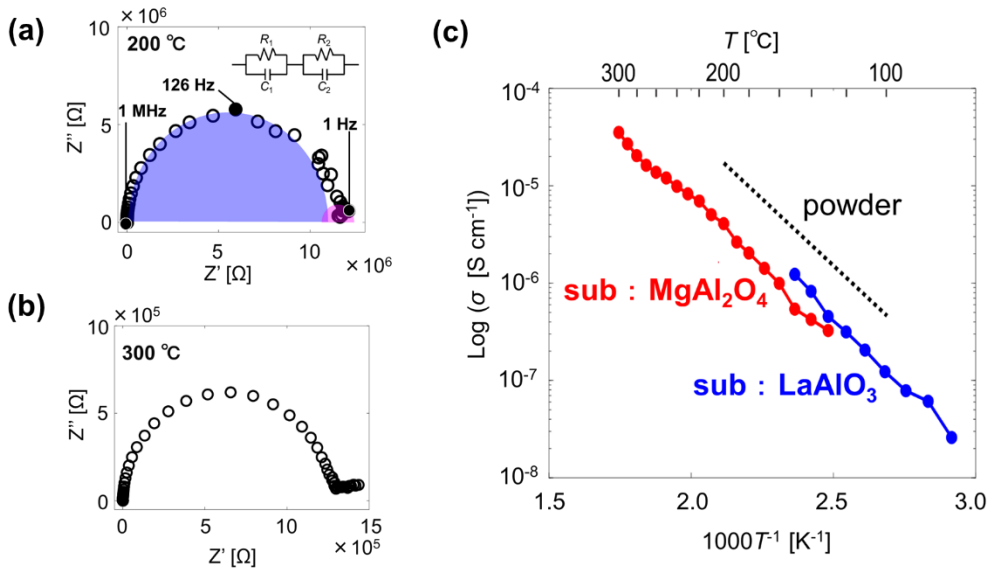

Figure 7. (a) A Nyquist plot obtained at 200 °C for the $SrLiH_3$ epitaxial thin film deposited on a $MgAl_2O_4$ (100) substrate. The blue and pink semicircles were obtained by circle fitting of the Nyquist plot. A capacitance value calculated from the blue semicircle was 1.1×10^{-10}, indicating that the semicircle was for the hydride-ion conduction of $SrLiH_3$ crystal grains. In the same way, the pink semicircle with a capacitance value of 3.2×10^{-8} F indicated that it was for the grain boundary. (b) A Nyquist plot obtained at 300 °C. (c) Hydride-ion conductivity of $SrLiH_3$ crystal grains determined by the Nyquist plots obtained at different temperatures. The conductivity of the film grown on the $MgAl_2O_4$ and $LaAlO_3$ substrates are colored in red and blue, respectively. The black dashed line corresponds to conductivity of $SrLiH_3$ powder reported in the previous study.[15]

the peak intensity was higher on the lattice-matched $LaAlO_3$ substrate than $MgAl_2O_4$. The half-width of the rocking curve was also greatly affected by the lattice matching between the films and substrates, with the half-widths of 0.74° and 2.38° for the LAO and $MgAl_2O_4$ substrates, respectively (Figure 6(c) and (d)). The h00 diffraction peak of the films on the $LaAlO_3$ substrate was more dominant than that on the $MgAl_2O_4$ substrate, indicating that the (100) orientation of the films was also higher. In the XRD φ scan profiles, the 111 diffraction peaks appeared at the same rotation angle for the $SrLiH_3$ films and the substrates, indicating that the in-plane epitaxial relationship is $[001]_{SrLiH3} \parallel [001]_{sub}$ (Figure 6(e) and (f)). SEM observations and EDS measurements of the film cross section confirmed that the $SrLiH_3$ film, similarly for the $BaLiH_3$ film, was a uniform and dense film suitable for the evaluation of hydride-ion conduction (Figure S3). The LiH 200 diffraction peak observed in the $BaLiH_3$ film was again observed in the $SrLiH_3$ films.

Finally, the hydride-ion conductivity of $SrLiH_3$ epitaxial films was evaluated by electrochemical impedance method to demonstrate that the intrinsic hydride-ion conduction of the material can be observed with the epitaxial films. The reason why we chose $SrLiH_3$ epitaxial films here is that it is known to exhibit higher hydride-ion conductivity than $BaLiH_3$.[15] Figure 7(a) shows the Nyquist plot obtained by measurement at 200 °C. Except for a slight deviation on the low frequency side, the plot was ideal semi-circular. This result contrasted with the earlier report for the $SrLiH_3$ powder.[15] The capacitance value calculated from the data analysis (circle fitting) is 1.1×10^{-10} F, which confirms that we are indeed observing hydride-ion conduction[15] within the crystal grains. Fitting to the low-frequency side of the Nyquist plot yielded a capacitance value of 3.2×10^{-8} F, suggesting hydride-ion conduction at the grain boundary. The Nyquist plot obtained by measurement at 300 °C (Figure 7(b)) showed a straight line in the low-frequency region suggesting hydride-ion diffusion at the electrode interface. The intrinsic hydride-ion conductivity of the $SrLiH_3$ crystal was determined by fitting Nyquist plots obtained in the temperature range from 70 °C to 300 °C (Figure 7(c)). The hydride-ion conductivity σ was 2.6×10^{-8} S cm^{-1} at 70 °C and 4.4×10^{-5} S cm^{-1} at 300 °C, about one-fifth lower than in the powder study. The activation energy was about 57 kJ mol^{-1}, which was similar to the powder study.[15] Comparing films on different substrates ($MgAl_2O_4$ and $LaAlO_3$), the conductivity was almost the same, indicating that the epitaxial films enables us to accurately evaluate the hydride-ion conductivity of perovskite hydrides even if their crystallinity differs slightly.

4. CONCLUSION

In this study, epitaxial thin films of $BaLiH_3$ and $SrLiH_3$ were successfully synthesized by using radical hydrogen reactive infrared laser evaporation. The success verified that radical hydrogen promoted the reaction between the metal and hydrogen during film growth and played an essential role for obtaining high-quality perovskite hydride epitaxial thin films. For the $SrLiH_3$ epitaxial thin film, electrochemical impedance measurements were performed. The shape of the obtained Nyquist plots was almost semicircular, corresponding to hydride-ion conduction in the $SrLiH_3$ crystal. This result demonstrated that intrinsic hydride-ion conduction can be evaluated using the epitaxial thin film. Conductivity of the $SrLiH_3$ epitaxial thin film was about one-fifth of the value reported in the powder study. In the future, this study may lead to the synthesis of epitaxial thin films of various hydrides. In addition, the intrinsic physical properties of perovskite hydrides will be elucidated using epitaxial

thin films. Understanding of intrinsic physical properties will shed light on its origin and facilitate material design research of the perovskite hydrides, which should construct basis for the development of innovative functional materials that exhibit hydrogen-derived unique properties.

ASSOCIATED CONTENT

Electrochemical impedance measurement technique, additional XRD data, crystal structure, SEM images. These materials are available free of charge via the Internet at http://pubs.acs.org.

AUTHOR INFORMATION

Corresponding Author

Department of Applied Chemistry, Graduate School of Engineering and Science, Shibaura Institute of Technology, 3-7-5 Toyosu, Koto-ku, Tokyo, Japan
E-mail: h-oguchi@shibaura-it.ac.jp

Author Contributions

E.F. and H.O. planned the experiments; E.F. performed synthesis, evaluation, and data analysis; F.M. and K.M. assisted with synthesis; and T.H. assisted with XRD measurements. All authors discussed the results and commented on the manuscript.

Funding Sources

Grant-in-Aid for Challenging Exploratory Research (7K19 K22225), the 56th Kowa Lithium Award from the Liberace Research Fund, the S-SPIRE project at Shibaura Institute of Technology, and the NIMS Collaboration Center Promotion Program (2022-87) (2023-024).

ACKNOWLEDGMENT

This work was supported by Grant-in-Aid for Challenging Exploratory Research (7K19 K22225), the 56th Kowa Lithium Award from the Liberace Research Fund, the S-SPIRE project at Shibaura Institute of Technology, and the NIMS Collaboration Center Promotion Program (2022-87) (2023-024). We thank Associate Professor Masaki Nakano of the Quantum Phase Electronics Research Center, Department of Physics and Engineering, Graduate School of Engineering, the University of Tokyo for his assistance with XRD measurements. Dr. Kyosuke Matsushita and Dr. Makiko Oshida of the Battery Research Platform, National Institute for Materials Science (NIMS) for their assistance with AFM and SEM measurements, and Dr. Masatomo Sumiya of the National Institute for Materials Science (NIMS) for development of a radical hydrogen generator.

REFERENCES

(1) Orimo, S.; Nakamori, Y.; Eliseo, J. R.; Züttel, A.; Jensen, C. R. Complex Hydrides for Hydrogen Storage. *Chem. Rev.* **2007**, *107*, 4111.

(2) Schlapbach, L.; Züttel, A. Hydrogen-storage materials for mobile applications. Nature **2001**, *414*, 353-358.

(3) Drozdov, A. P.; Kong, P. P.; Minkov, V. S.; Besedin, S. P.; Kuzovnikov, M. A.; Mozaffari, S.; Balicas, L.; Balakirev, F. F.; Graf, D. E.; Prakapenka, V. B.; et al. Superconductivity at 250 K in lanthanum hydride under high pressures. *Nature* **2019**, *569*, 528-531.

(4) Verbraeken, M. C.; Cheung, C.; Suard, E.; Irvine, J. T. High H- ionic conductivity in barium hydride. *Nat Mater* **2015**, *14*, 95-100.

(5) Ashcroft, N. W. Metallic Hydrogen: A High-Temperature Superconductor? *Phys. Rev. Lett.* **1968**, *21*, 1748.

(6) Richardson, F. C.; Ashcroft, N. W. High Temperature Superconductivity in Metallic Hydrogen: Electron-Electron Enhancements. *Phys. Rev. Lett.* **1997**, *78*, 118.

(7) Verbraeken, M. C.; Cheung, C.; Suard, E.; Irvine, J. T. High H- ionic conductivity in barium hydride. *Nat Mater* **2015**, *14*, 95-100.

(8) Ubukata, H.; Takeiri, F.; Shitara, K.; Tassel, C.; Saito, T.; Kamiyama, T.; Broux, T.; Kuwabara, A.; Kobayashi, G.; Kageyama, H. Anion ordering enables fast H− conduction at low temperatures. *Sci. Adv.* **2021**, *7*, eabf7883.

(9) Messer, C. E.; Eastman, J. C.; Mers, R. G.; Maeland. A. J. Ternary Perovskite Phases in Systems of Lithium Hydride with Barium, Strontium, and Calcium Hydrides. *Inorg. Chem.* **1964**, *3*, 776-778.

(10) Yalcin, B. G.; Salmankurt, B.; Duman, S. Investigation of structural, mechanical, electronic, optical, and dynamical properties of cubic $BaLiF_3$, $BaLiH_3$, and $SrLiH_3$. *Mater.* **2016**, *3*, 036301.

(11) Raza, H. H.; Murtaza, G.; Umm-e-Hani; Arif Khalil, R. M. Optoelectronic and thermal properties of LiXH$_3$(X =Ba, Sr and Cs) for hydrogen storage materials: A first principle study. *Solid State Commun.* **2019**, *299*, 113659

(12) Wiedemann, D.; Heppke, E. M.; Franz, A. And Yet It Moves: A High‐Temperature Neutron Diffraction Study of Ion Diffusion in the Inverse Perovskites BaLiX_3 (X = F, H, D). *Eur. J. Inorg* **2019**, *2019*, 5085-5088.

(13) Shah, M. A. H.; Alam, M. A.; Hossain, A.; Hossain, M. F.; Nuruzzaman, M.; Parvin, F.; Zilani, M. A. K. Hydrostatic pressure on XLiH$_3$ (X = Ba, Sr, Ca) perovskite hydrides: An insight into structural, thermo-elastic and ultrasonic properties through first-principles investigation. *Solid State Commun.* **2021**, *328,* 114222.

(14) Schouwink, P.; Ley, M. B.; Tissot, A.; Hagemann, H.; Jensen, T. R.; Smrcok, L.; Cerny, R. Structure and properties of complex hydride perovskite materials. *Nat Commun* **2014**, *5*, 5706.

(15) Hirose, T.; Mishina, T.; Matsui, N.; Suzuki, K.; Saito, T.; Kamiyama, T.; Hirayama, M.; Kanno, R. Fast Hydride-Ion Conduction in Perovskite Hydrides AELiH$_3$. *ACS Appl. Energy Mater.* **2022**, *5*, 2968-2974.

(16) Nishio, K.; Imazeki, D.; Kurushima, K.; Takeda, Y.; Edamura, K.; Nakayama, R.; Shimizu, R.; Hitosugi, T. Immense Reduction in Interfacial Resistance between Sulfide Electrolyte and Positive Electrode. *ACS Appl. Mater. Interfaces* **2022**, *14*, 34620-34626.

(17) Wildes, A.R.; Ward, R.C.C.; Wells, M.R.; Hjörvarsson, B. The formation of epitaxial YH_2 in MBE grown yttrium thin films with a thin gold capping layer. *J. Alloys Compd.* **1996**, *242*, 49–57.

(18) Udovic, T. J.; Huang, Q.; Erwin, R. W.; Hjörvarsson, B.; Ward. R. C. C. Structural symmetry of YD_3 epitaxial thin films. *Phys. Rev. B* **2000**, *61*, 12701.

(19) Tessier, P.; Fruchart, D.; Givord. D. Magnetic properties of epitaxial gadolinium hydride films. *J. Alloys Compd.* **2002**, *330-332*, 369–372.

(20) Oguchi, H.; Ikeshoji, T.; Ohsawa, T.; Shiraki, S.; Kuwano, H.; Orimo, S.; Hitosugi, T. Epitaxial thin film growth of LiH using a liquid-Li atomic template. *Appl. Phys. Lett.* **2014**, *105*, 211601

(21) Oguchi, H.; Isobe, S.; Kuwano, H.; Shiraki, S.; Orimo, S.-i.; Hitosugi, T. Pulsed laser deposition of air-sensitive hydride epitaxial thin films: LiH. *APL Mater.* **2015**, *3*, 096106.

(22) Yoshimatsu, K.; Suzuki, T.; Tsuchimine, N.; Horiba, K.; Kumigashira, H.; Oshima, T.; Ohtomo, A. Direct growth of metallic TiH_2 thin films by pulsed laser deposition. *Appl. Phys. Express* **2015**, *8*, 035801.

(23) Shimizu, R.; Sasahara, Y.; Oguchi, H.; Yamamoto, K.; Sugiyama, I.; Shiraki, S.; Orimo, S.; Hitosugi, T. Fabrication of atomically abrupt interfaces of single-phase TiH_2 and Al_2O_3. *APL Mater.* **2017**, *5*, 086102.

(24) Shimizu, R.; Kakinokizono, T.; Gu, I.; Hitosugi, T. Epitaxial Growth of Single-Phase Magnesium Dihydride Thin Films. *Inorg Chem* **2019**, *58*, 15354-15358.

(25) Sasahara, Y.; Shimizu, R.; Oguchi, H.; Nishio, K.; Ogura, S.; Morioka, H.; Orimo, S.; Fukutani, K.; Hitosugi, T. A hysteresis loop in electrical resistance of NbH_x observed above the β-λ transition temperature. *AIP Adv.* **2019**, *9*, 015027.

(26) Hasegawa, N.; Kawasoko, H.; Fukumura T. Direct Growth and Electrical Properties of YH_2 (111) Epitaxial Thin Films on CaF_2 (111) and (001) Substrates by Reactive Magnetron Sputtering. *Chem. Lett*. **2020**, *49*, 1181-1184.

(27) Komatsu, Y.; Shimizu, R.; Wilde, M.; Kobayashi, S.; Sasahara, Y.; Nishio, K.; Shigematsu, K.; Ohtomo, A.; Fukutani, K.; Hitosugi, T. Epitaxial Thin Film Growth of Europium Dihydride. *Cryst. Growth* **2020**, *20*, 5903-5907.

(28) Oguchi, H.; Kim, S.; Maruyama, S.; Horisawa, Y.; Takagi, S.; Sato, T.; Shimizu, R.; Matsumoto, Y.; Hitosugi, T.; Orimo, S.-i. Epitaxial Film Growth of $LiBH_4$ via Molecular Unit Evaporation. *ACS ACS Appl. Electron. Mater.* **2019**, *1*, 1792-1796.

(29) Nakayama, R.; Kawaguchi, Y.; Shimizu, R.; Nishio, K.; Oguchi, H.; Kim, S.; Orimo, S.; Hitosugi, T. Fabrication and Growth Orientation Control of $NaBH_4$ Epitaxial Thin Films Using Infrared Pulsed-Laser Deposition. *Cryst.* **2022**, *22* , 6616-6621.

(30) Takeyama, Y.; Maruyama, S.; Matsumoto, Y. Development of compact CW-IR laser deposition system for high-throughput growth of organic single crystals. *Sci. Technol. Adv. Mater.* **2011**, *12*, 054210.

(31) Dahmani, F. Z.; Okamoto, Y.; Tsutsumi, D.; Ishigaki, T.; Koinuma, H.; Hamzaoui, S.; Flazi, S.; Sumiya, M. Density evaluation of remotely-supplied hydrogen radicals produced via tungsten filament method for $SiCl_4$ reduction. *Jpn. J. Appl. Phys.* **2018**, *57*, 051301.

(32) Okamoto, Y.; Sumiya, M.; Nakamura, Y.; Suzuki, Y. Effective silicon production from $SiCl_4$ source using hydrogen radicals generated and transported at atmospheric pressure. *Sci. Technol. Adv. Mater.* **2020**, *21*, 482-491.

(33) Karazhanov, S. Zh.; Ulyashin, A. G.; Vajeeston, P.; Ravindran, P. Hydrides as materials for semiconductor electronics. *Philos. Mag.* **2008**, *88*, 2461–2476.

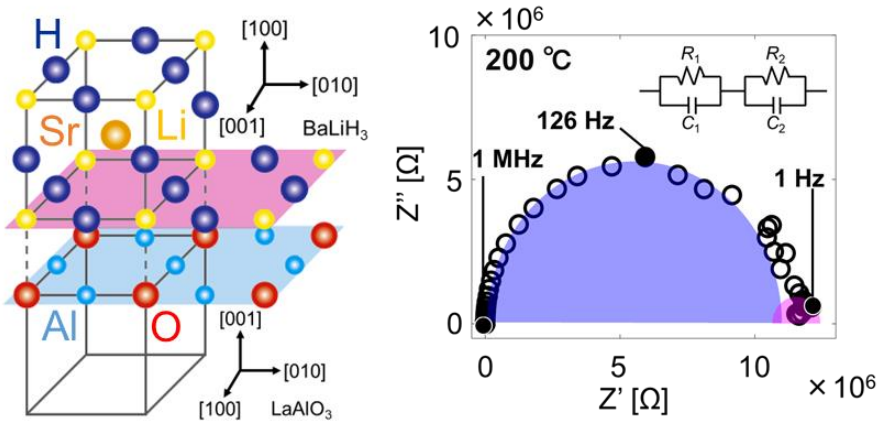

Insert Table of Contents artwork here